Highly Efficient Light-Emitting Diodes Based on Fluorene Copolymer Consisting of Triarylamine Units in the Main Chain and Oxadiazole Pendent Groups

Fang-Iy Wu, Ping-I Shih, and Ching-Fong Shu*

Department of Applied Chemistry, National Chiao Tung University, 300, Hsinchu, Taiwan

Yung-Liang Tung and Yun Chi*

Department of Chemistry, National Tsing Hua University, 300, Hsinchu, Taiwan

Received August 22, 2005

ABSTRACT: We have synthesized a fluorene-based copolymer, PFA-OXD, which possesses bipolar charge-transporting functionalities, through the incorporation of electron-rich triphenylamine moieties and electron-deficient oxadiazole pendent groups into the polymer backbone and onto the C9 position of each fluorene repeating unit, respectively. The propeller-shaped triphenylamine units in the main chain and the rigid cardo-type OXD side chains endow this polymer with a very high glass transition temperature (306 °C) and good thermal stability, without sacrificing its good solution processability. Both in dilute solution and as a thin film, PFA-OXD exhibits a bright blue emission upon excitation of either the main chain or oxadiazole side chains; this phenomenon indicates that efficient energy transfer occurs from the photoexcited pendent groups to the polymer backbone. An organic light-emitting device incorporating this copolymer as the emitting layer exhibits a voltage-independent and stable blue emission having color coordinates (0.14, 0.15) at 9 V; the maximum brightness was 7128 cd m^{-2} and the maximum luminance efficiency was 2.07 cd A^{-1}. In addition, doping PFA-OXD as a host material with 2.6 wt % of a red-emitting phosphorescent dye, Os(fppz), led to a high-brightness, highly efficient red electroluminescent device having CIE coordinates of (0.65, 0.34), a maximum brightness of 28 440 cd m^{-2}, and a maximum external efficiency of 9.30%.

Introduction

Conjugated polymer light-emitting diodes (PLEDs) have attracted considerable interest because of their potential applications in flat-panel displays.[1,2] Solution processing of semiconductor polymers has the advantage of allowing spin-coating and printing methods to be utilized for the preparation of large-area-display devices. In addition, PLEDs offer the flexibility of fine-tuning the luminescent properties of the device through manipulation of chemical structures. Many conjugated polymers whose emission wavelengths can be tuned to span the entire visible spectrum range—through simple copolymerization of appropriate monomers—have been synthesized as components of potential polymer-based LEDs.[3] Polymers having large band gaps so that they emit blue light efficiently are of particular interest because they can be used either as blue light sources in full-color displays or as host materials for lower energy fluorescent or phosphorescent dyes.[4]

Because of their high photoluminescence (PL) and electroluminescence (EL) efficiencies, polyfluorenes (PFs) are promising materials for blue light emitting diodes.[5] Nevertheless, there are some drawbacks that continue to hamper their potential applicability, especially the undesired green emission that appears upon thermal annealing or device operation. This low-energy emission band has been attributed to the formation of excimers or aggregates in the solid state.[6] Several approaches have been described for the suppression of excimer or aggregate formation, including the attachment of sterically hindered side groups at the C9 position of fluorene units[7] and the introduction of disorder into the π-conjugated system of the rigid-rod backbone of PFs.[8] An alternative explanation for the formation of the green emission is that it is caused by keto defects arising from oxidation at the C9 positions of fluorene units that have not been fully alkylated.[9] If this is the case, purification of monomers to a high degree prior to their polymerization is required to avoid the formation of the keto defects.

Another problem for PFs in PLED applications is their high ionization potential (5.8 eV);[10] i.e., a high-energy barrier exists for holes to travel into the PFs from the indium tin oxide (ITO)/poly(3,4-ethylenedioxythiophene) (PEDOT) layer (5.2 eV),[11] which results in higher driving voltages.[7a] Although blends prepared by doping PFs with hole-transporting molecules have led to some improvement in hole injection from the anode, as well as EL stability,[12] physical blending of these small molecules into polymeric hosts runs the risk of phase separation occurring over time. The incorporation of electron-rich tertiary aromatic amines into polyfluorene backbones can lead to copolymers having lower ionization potentials (5.0−5.3 eV)[13] that are better matched with the work function of the ITO/PEDOT layer (5.2 eV). Consequently, devices based on these copolymers exhibit lower operating voltages relative to those of devices based on the corresponding fluorene homopolymers.[14] Moreover, the hole mobility of such fluorene−triarylamine copolymers can reach as high as 3×10^{-3} cm^2 V^{-1} s^{-1} (at a bias field of 2.5×10^5 V cm^{-1}), which is about 1 order of magnitude higher than that of poly(9,9-dioctylfluorene) (POF) and is comparable to that of the widely used hole-transporting molecule *N*,*N*′-diphenyl-*N*,*N*′-bis(3-methylphenyl)-1,1-biphenyl-4,4′-diamine (TPD).[15]

10.1021/ma051842r CCC: $30.25 © 2005 American Chemical Society
Published on Web 09/30/2005

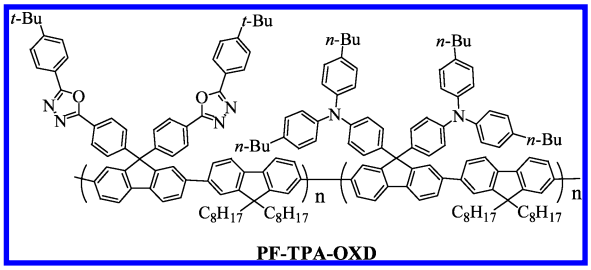

Figure 1. Chemical structure of PF-TPA-OXD, a polyfluorene possessing both hole- and electron-transporting moieties as side chains.

Scheme 1. Synthesis of PFA-OXD[a]

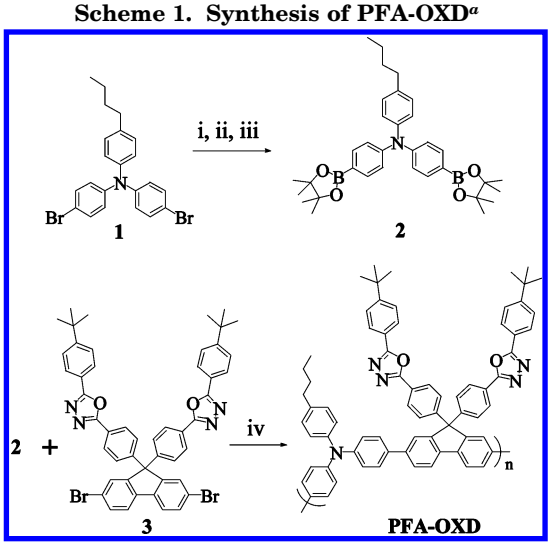

[a] Reagents: (i) *n*-BuLi/THF, $B(OMe)_3$; (ii) 2 N HCl; (iii) pinacol/benzene; (iv) $Pd(PPh_3)_4/K_2CO_3$, toluene/H_2O/Aliquat 336.

To achieve high electroluminescent efficiency, it is necessary to balance the transport of electrons and holes. Previously, we achieved balanced charge recombination in electroluminescent devices by utilizing PF-TPA-OXD,[7c] a fluorene-based copolymer possessing both hole- and electron-transporting moieties as side chains (Figure 1). This blue fluorene-based copolymer is also a very promising candidate for use as a host material in molecularly doped electrophosphorescence devices because of its wide energy gaps and large numbers of charge-transporting pendent groups, which improve the confinement of triplet excitons in the phosphorescent dopants and provide efficient charge transportation, respectively.[4h-l] In this study, we introduced electron-deficient oxadiazole (OXD) groups as pendent units to compensate for the poor electron-transporting ability of a p-type fluorene−triarylamine copolymer. Scheme 1 depicts the chemical structure of PFA-OXD, which possesses bipolar transport properties; we prepared it through Suzuki coupling copolymerization. Instead of the deep-blue emission of typical PFs that occurs at 425 nm, the emission maximum of PFA-OXD is red-shifted to 461 nm; i.e., it is located in the blue region where the human eye is more sensitive. PFA-OXD has the attractive feature of possessing a high content of OXD groups—to raise the electron-transporting capability efficiently—while retaining the integrity of the optical properties of the polymer backbone because of the interrupted π-conjugation, between the pendent OXD units and the polymer backbone, caused by the C9 atom of each substituted fluorene unit. Moreover, we expected that the presence of these sterically demanding pendent groups may also prevent the occurrence of π-stacking between polymer chains and suppress the formation of excimers in the solid state.[7] We observed a bright and stable blue electroluminescence from a device prepared using PFA-OXD as the emitting layer. Furthermore, we also obtained high-performance red-electrophosphorescent devices displaying a high current and luminance when employing PFA-OXD as the polymeric host and Os(fppz) as an efficient red phosphor.[16]

Experimental Section

Materials. 4-Butyl-*N*,*N*-diphenylaniline,[17] monomer **3**,[7b] Os(fppz),[16] and the electron-transporting material 1,3,5-tris(*N*-phenylbenzimidazol-2-yl)benzene (TPBI)[18] were prepared according to reported procedures. The solvents were dried using standard procedures. All other reagents were used as received from commercial sources, unless otherwise stated.

Characterization. ^1H and ^{13}C NMR spectra were recorded on Varian UNITY INOVA AS500 (500 MHz) and Bruker-DRX 300 (300 MHz) spectrometers. Mass spectra were obtained using a JEOL JMS-HX 110 mass spectrometer. Size exclusion chromatography (SEC) was performed using a Waters chromatography unit interfaced with a Waters 410 differential refractometer; three 5-μm Waters styragel columns (300 × 7.8 mm) were connected in series in order of decreasing pore size (10^4, 10^3, and 10^2 Å); tetrahydrofuran (THF) was the eluent. Standard polystyrene samples were used for calibration. Differential scanning calorimetry (DSC) was performed using a SEIKO EXSTAR 6000DSC unit at a heating rate of 20 °C min^{-1} and a cooling rate of 40 °C min^{-1}. Samples were scanned from 30 to 370 °C, cooled to 0 °C, and then scanned again from 30 to 370 °C. The glass transition temperatures (T_g) were determined from the second heating scan. Thermogravimetric analysis (TGA) was undertaken using a DuPont TGA 2950 instrument. The thermal stabilities of the samples were determined under nitrogen atmosphere by measuring their weight loss while heating at a rate of 20 °C min^{-1}. UV−vis spectra were measured using an HP 8453 diode-array spectrophotometer. PL spectra were obtained from a Hitachi F-4500 luminescence spectrometer. Cyclic voltammetry (CV) measurements were performed using a BAS 100 B/W electrochemical analyzer in anhydrous acetonitrile containing 0.1 M tetrabutylammonium hexafluorophosphate ($TBAPF_6$) as the supporting electrolyte at a scan rate of 100 mV s^{-1}. The potentials were measured against an Ag/Ag^+ (0.01 M $AgNO_3$) reference electrode using ferrocene as the internal standard. The onset potentials were determined from the intersection of two tangents drawn at the rising and background currents of the cyclic voltammogram. Atomic force microscopy measurements were undertaken in the tapping mode using a Digital Nanoscope IIIa instrument under ambient conditions.

Fabrication of Light-Emitting Devices. LED devices were fabricated in the structure indium tin oxide (ITO)/poly(styrenesulfonate)-doped poly(3,4-ethylenedioxythiophene) (PEDOT) (35 nm)/polymer emitting layer (50−70 nm)/TPBI (30 nm)/Mg:Ag (100 nm)/Ag(100 nm). The PEDOT was spin-coated directly onto the ITO glass and dried at 80 °C for 12 h under vacuum to improve both hole injection and the substrate's smoothness. The light-emitting layer was spin-coated on top of the PEDOT layer using chlorobenzene as the solvent, and then the sample was dried for 3 h at 60 °C under vacuum. Prior to film casting, the polymer solution was filtered through a Teflon filter (0.45 μm). The TPBI layer, which was used as an electron-transporting layer that would also block holes and confine excitons, was grown by thermal sublimation in a vacuum of 3×10^{-6} Torr.[19] Subsequently, the cathode, Mg:Ag (10:1, 100 nm) alloy, was deposited by coevaporation onto the TPBI layer; this process was followed by placing an additional layer of Ag (100 nm) onto the alloy as a protection layer. The current−voltage−luminance relationships were measured under ambient conditions using a Keithley 2400 source meter and a Newport 1835C optical meter equipped with an 818ST silicon photodiode.

4-Butyl-*N*,*N*-bis(4-bromophenyl)aniline (1). A mixture of 4-butyl-*N*,*N*-diphenylaniline (0.93 g, 3.09 mmol) and $CuBr_2$/Al_2O_3 (10.0 g)[20] in CCl_4 (25 mL) was heated at 60 °C for 2 h. The solid part was removed by filtration and washed with CCl_4. The solvent was evaporated from the combined filtrate under reduced pressure. The crude product was purified by column chromatography, eluting with hexane to give a colorless liquid (0.93 g, 65.5%). ^{1}H NMR (300 MHz, $CDCl_3$): δ 0.93 (t, J = 7.4 Hz, 3H), 1.31−1.43 (m, 2H), 1.53−1.64 (m, 2H), 2.57 (t, J = 7.5 Hz, 2H), 6.90 (d, J = 8.6 Hz, 4H), 6.96 (d, J = 8.3 Hz, 2H), 7.08 (d, J = 8.3 Hz, 2H), 7.30 (d, J = 8.6 Hz, 4H). ^{13}C NMR (75 MHz, $CDCl_3$): δ 14.0, 22.4, 33.6, 35.0, 114.9, 124.9, 125.0, 129.5, 132.2, 138.8, 144.4, 146.7. MS: *m/z* 459 $[M]^+$.

Synthesis of Monomer 2. *n*-Butyllithium in hexane (2.5 M, 8.0 mL) was added slowly under nitrogen to a stirred solution of 4-butyl-*N*,*N*-bis(4-bromophenyl)aniline (**1**, 3.70 g, 8.06 mmol) in THF (30 mL) at −78 °C, and then the mixture was stirred for 1 h at this temperature. Trimethyl borate (2.2 mL, 19.4 mmol) was added at −78 °C, and then the mixture was warmed slowly to room temperature and stirred for another 1 h. The reaction mixture was poured into 2 N HCl (100 mL) and stirred overnight, followed by extraction with ether and drying ($MgSO_4$). Concentration under reduced pressure gave the corresponding diboronic acid, which, without further purification, was reacted with pinacol (1.00 g, 8.47 mmol) in benzene under reflux overnight using a Dean−Stark trap to effect condensation through the azeotropic removal of water. The resulting residue was passed through a short column (silica gel; EtOAc) and purified by recrystallization from THF/hexane (1:8) to afford **2** (2.18 g, 49.0%). ^{1}H NMR (300 MHz, $CDCl_3$): δ 0.92 (t, J = 7.3 Hz, 3H), 1.27−1.39 (m, 26 H), 1.56−1.61 (m, 2H), 2.56 (t, J = 7.6 Hz, 2H), 7.00 (d, J = 8.6 Hz, 2H), 7.03 (d, J = 8.6 Hz, 4H), 7.07 (d, J = 8.6 Hz, 2H), 7.64 (d, J = 8.6 Hz, 4H). ^{13}C NMR (75 MHz, $CDCl_3$): δ 14.0, 22.4, 24.8, 33.6, 35.1, 83.6, 122.4, 125.8, 129.3, 135.8, 138.9, 144.5, 150.2. HRMS $[M]^+$: calcd for $C_{34}H_{45}B_2NO_4$, *m/z* 553.3535; found, 553.3536. Anal. Calcd for $C_{34}H_{45}B_2NO_4$: C, 73.80; H, 8.20; N, 2.53. Found: C, 73.50; H, 8.36; N, 2.87.

PFA-OXD. Aqueous K_2CO_3 (2.0 M, 5.0 mL) and Aliquat 336 (ca. 70 mg) were added to a mixture of monomer **2** (253 mg, 456 μmol) and **3** (400 mg, 456 μmol) in toluene (8.0 mL). The mixture was degassed; then tetrakis(triphenylphosphine)-palladium (10 mg, 1.9 mol %) was added in one portion under N_2, and then the solution was heated at 110 °C for 72 h. The end groups were capped by heating the mixture under reflux for 12 h with benzeneboronic acid (130 mg, 1.07 mmol) and then for 12 h with bromobenzene (170 mg, 1.07 mmol). The reaction mixture was cooled to room temperature and precipitated into a mixture of MeOH and H_2O (2:1 v/v, 150 mL). The crude polymer was collected, washed with excess MeOH, dissolved in chloroform, and then reprecipitated twice into MeOH. Finally, the polymer was washed with acetone for 48 h using a Soxhlet apparatus and then dried under vacuum to give PFA-OXD (326 mg, 70.4%). ^{1}H NMR (500 MHz, $CDCl_3$): δ 0.88−0.93 (m, 3H), 1.27−1.38 (m, 20H), 1.53−1.61 (m, 2H), 2.53−2.57 (m, 2H), 7.01−7.09 (m, 4H), 7.09−7.14 (m, 4H), 7.39−7.48 (m, 8H), 7.48−7.53 (m, 4H), 7.59 (s, 2H), 7.62−7.65 (m, 2H), 7.82−7.86 (m, 2H), 7.95−8.06 (m, 8H). ^{13}C NMR (125 MHz, $CDCl_3$): δ 14.0, 22.4, 31.1, 33.6, 35.0, 65.7, 120.8, 121.0, 122.7, 123.6, 124.0, 125.2, 126.0, 126.7, 127.1, 127.7, 128.8, 129.3, 134.5, 138.6, 138.7, 140.6, 144.7, 147.2, 149.2, 150.6, 155.3, 164.0, 164.6. Anal. Calcd for $C_{71}H_{61}N_5O_2$: C, 83.91; H, 6.05; N, 6.89. Found: C, 82.83; H, 6.14; N, 6.56.

Results and Discussion

Synthesis. Scheme 1 displays the synthetic route we used to prepare monomer **2** and the fluorene−triphenylamine copolymer (PFA-OXD). Compound **1** was synthesized by bromination of 4-butyl-*N*,*N*-diphenylaniline with alumina-supported copper(II) bromide.[20] The lithiation of **1** with *n*-BuLi, followed by treatment with trimethyl borate and hydrolysis in aqueous HCl, gave the corresponding boronic acid, which, without further purification, we converted to the boronic ester **2** upon reaction with pinacol. We synthesized the alternating copolymer PFA-OXD containing oxadiazole pendent groups through Suzuki polymerization of equimolar amounts of the diboronate monomer **2** and the dibromo monomer **3**, using $Pd(PPh_3)_4$ as the catalyst, in a mixture of toluene and aqueous K_2CO_3 (2.0 M) in the presence of Aliquat 336 as a phase transfer reagent.[21]

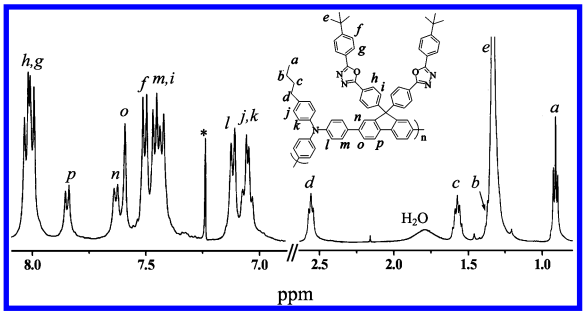

Figure 2. ^{1}H NMR spectrum (500 MHz, $CDCl_3$) of PFA-OXD in $CDCl_3$. The asterisk indicates the signal arising from $CHCl_3$.

We used ^{1}H and ^{13}C NMR spectroscopy to verify the chemical structure of the copolymer. Figure 2 presents a representative ^{1}H NMR spectrum of PFA-OXD in $CDCl_3$. In the aliphatic region, we assign the resonances at δ 0.91, 1.35, 1.57, and 2.55 to the aliphatic protons of the *n*-butyl chains attached to the triphenylamine units of PFA-OXD, with the intense peak centered at 1.33 ppm representing the methyl group protons of the *tert*-butyl substituent on the OXD pendent groups. We established the chemical shift assignments of the aromatic protons from detailed analyses of the ^{1}H and ^{13}C NMR spectroscopic data, aided by two-dimensional ^{1}H−^{1}H correlation spectra (^{1}H−^{1}H COSY) and long-range ^{1}H−^{13}C heteronuclear correlation spectra (HMBC). In the ^{13}C NMR spectrum, we ascribe the signal at 65.7 ppm, which superimposes with the signal of the C9 carbon atom of monomer **3**, to the C9 carbon atom of the fluorene repeating units in the copolymer. We employed size exclusion chromatography (SEC), using THF as the eluent and calibrating against polystyrene standards, to determine the molecular weight of the polymer. PFA-OXD possesses a weight-average molecular weight (M_w) of ca. 3.8×10^4 g mol^{-1} and a polydispersity index of 2.4.

We investigated the thermal properties of PFA-OXD by performing thermogravimetric analysis (TGA) and differential scanning calorimetry (DSC) measurements. As indicated in Figure 3, PFA-OXD exhibits excellent thermal stability with the onset decomposition temperature at ca. 400 °C followed by a 5% weight loss occurring at 465 °C. In the DSC measurement, we observed a distinct glass transition at 306 °C, but detected no crystallizing or melting peaks at temperatures up to 370 °C (see the inset of Figure 3). On the other hand, the sample of POF prepared by rapid cooling from its molten state exhibited, in succession, a glass transition (T_g) at 67 °C, an exothermic crystallization peak at 94 °C, and a melting peak at 152 °C.[8c] It is evident that the presence of the propeller-like triphenylamine (TPA) units in PFA-OXD hinders close packing of the polymer chains and suppresses their crystallizability.[22] Moreover, the introduction of two rigid oxadiazole groups onto the C9 position of each fluorene repeating unit provided a three-dimensional cardo structure to enhance the chain rigidity of PFA-OXD and

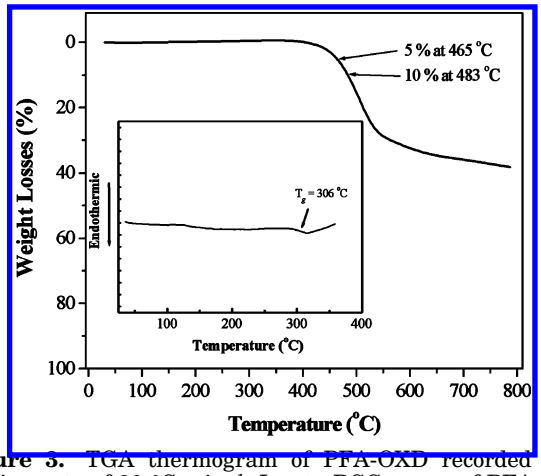

Figure 3. TGA thermogram of PFA-OXD recorded at a heating rate of 20 °C min^{-1}. Inset: DSC traces of PFA-OXD recorded at a heating rate of 20 °C min^{-1}.

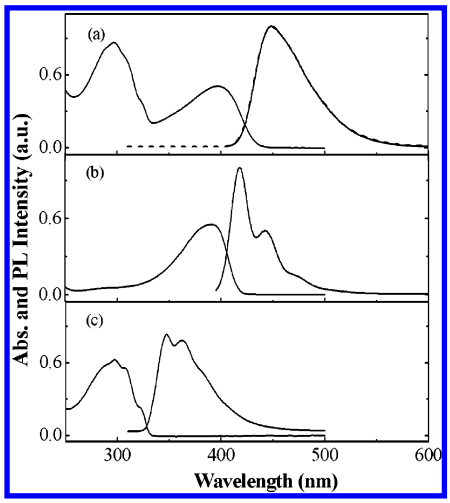

Figure 4. UV−vis absorption and PL spectra in THF solution of (a) PFA-OXD (solid and dashed lines, excited at 397 and 300 nm, respectively), (b) POF (excited at 391 nm), and (c) OXD (excited at 298 nm).

restrict its segmental mobility, which leads to its much higher value of T_g.[7b,c] In addition, the value of T_g of PFA-OXD is higher than that of PF-TPA-OXD (166 °C), because PF-TPA-OXD possesses additional 9,9-dioctylfluorene units in its main chain and four flexible *n*-butyl chains substituted on two triphenylamino pendent groups.[7c] Such a high value of T_g, which should prevent morphological changes from occurring and suppress the formation of aggregates and excimers upon exposure to heat, is desirable for polymers that are used as emissive materials for light-emitting applications. Although PFA-OXD has only short *n*-butyl chains functioning as solubilizing groups on the TPA unit, it is readily soluble in a broad range of organic solvents, such as chloroform, chlorobenzene, THF, and *N*-methyl-2-pyrrolidinone. Again, we attribute the high solubility of PFA-OXD to the presence of the propeller-shaped TPA units, which minimize interchain interactions between polymer chains.[22a,c,23]

Photophysical Properties. Figure 4 presents the UV−vis absorption and PL spectra of dilute solutions of PFA-OXD; Table 1 summarizes the spectral data. For the sake of comparison, Figure 4 also provides the absorption and PL spectra of POF and 2,5-di(4-*tert*-butylphenyl)-1,3,4-oxadiazole (OXD).[7b,c] In THF solution, PFA-OXD exhibits an absorption having its λ_{max} at 397 nm—it is red-shifted by only a few nanometers relative to that observed for POF—that we ascribe to a $\pi-\pi^*$ transition derived from the polymer backbone. An additional absorption band at 297 nm appears to arise mainly from the oxadiazole side chains because the model compound, OXD in THF, also has an absorption having λ_{max} at 298 nm. Upon excitation at 397 nm of the fluorene−triphenylamine main chain in THF, the PL displays an emission band at 449 nm. Although there is a moderate red shift with respect to that observed for the signal of POF (418 nm), the emission remains in the blue region and is closer to the maximum of a relative photopic luminous efficiency function than is the characteristic emission of POF.[24] We also noted that, in contrast to POF, which exhibits a vibronic fine structure, PFA-OXD exhibits a much less resolved PL spectrum. This loss of resolution reflects the lack of intrachain ordering that is due to the presence of propeller-like TPA segments in the polymer main chain.[25] As indicated in Figure 4, there is good spectral overlap between the emission band of the oxadiazole pendent units and the absorption band of the conjugated main chain of PFA-OXD, which meets the requirement for Förster energy transfer.[26] Accordingly, most of the excitons formed in the OXD pendent groups upon direct photoexcitation are likely to migrate to the fluorene−triphenylamine backbone, from which the emission occurs. Upon excitation of the OXD side groups at 300 nm, the PL spectrum (the dashed line drawn in Figure 4) is the same as that obtained when exciting the polymer backbone at 397 nm; in contrast, we detected no luminescence from the OXD side chains in the deep-blue region (350−400 nm). The fact that we observed complete quenching of the OXD emission even in a very dilute solution (10^{-6} M) indicates that efficient intramolecular energy transfer takes place in the PFA-OXD polymer and may contribute significantly to the emission intensity of the main chain. The PL quantum yield in THF, upon exciting at 365 nm, was 0.72, measured relative to 9,10-diphenylanthrancene ($\Phi_f = 0.9$) as a standard.[27]

In comparison with the results we obtained using dilute solutions, the absorption spectrum of the PFA-OXD thin film spin-coated from a chlorobenzene solution onto a quartz plate displays slight broadening, while the emission signal exhibits a red shift of 13 nm. We estimated the PL quantum yield of the PFA-OXD film to be 0.43 by comparing its fluorescence intensity to that of the POF polymer thin film sample that had been excited at 380 nm ($\Phi_f = 0.55$).[28] A key issue for the applicability of blue-emitting polymers is their spectral stability. The undesired green emission bands that often develop in PL and EL spectra of polyfluorenes have been attributed to physical (excimers or aggregates forma-

Table 1. Photophysical Properties of PFA-OXD, POF, and OXD

	solution[a]			film[b]		
	Abs (nm)	PL (nm)	Φ_f[c]	Abs (nm)	PL (nm)	Φ_f
PFA-OXD	297, 397	449[d]	0.72	300, 397	462[d]	0.43
POF	391	418		393	425	0.55[e]
OXD	298	347				

[a] Evaluated in THF. [b] Evaluated in the solid state and prepared from solutions in chlorobenzene. [c] Quantum yield (Φ_f) determined in THF, relative to 9,10-diphenylanthracence in cyclohexane (0.9), upon excitation at 365 nm. [d] Excited at 397 nm. [e] The thin film quantum efficiency of POF, as measured in an integrating sphere, was 0.55 (ref 28).

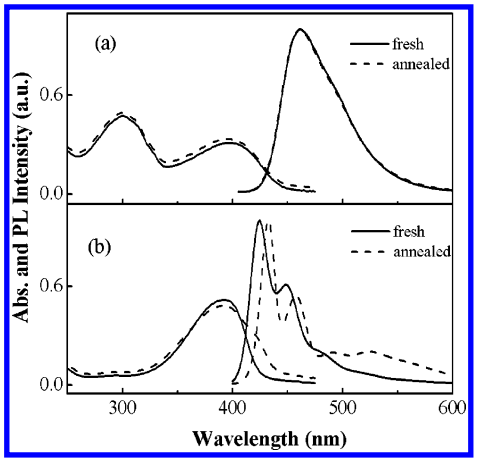

Figure 5. UV−vis absorption and PL spectra (excited at 380 nm) of (a) PFA-OXD and (b) POF films, recorded before and after annealing at 150 °C for 20 h under a nitrogen atmosphere.

tion) and chemical (keto defects) degradation processes.[6,9,29] To examine the color stability of PFA-OXD, we heated the polymer film for 20 h on a hot plate at 150 °C under a nitrogen atmosphere (Figure 5a). For the sake of comparison, we also prepared and annealed a thin film of POF under the same conditions. As displayed in Figure 5b, an additional absorption band at 423 nm appears for the POF film after annealing; the PL spectrum of the annealed film displays a moderate red shift with respect to the pristine film, together with the appearance of a long-wavelength emission band at 500−600 nm.[6] In contrast, the PL spectra of the PFA-OXD film remained intact—no long-wavelength tail appeared—after its thermal treatment. Thus, it is apparent that the thermal stability of PFA-OXD is improved significantly over that of POF as a result of the incorporation of TPA units into the PF backbone, which results in a twisted backbone conformation that, consequently, suppresses the π-stacking of polymer chains. In addition, the presence of the sterically demanding, rigid OXD pendent groups, which form three-dimensional cardo structures, further restricts close packing of the polymer chains and reduces the probability of interchain interactions; thus, the tendency to form aggregates and excimers in the polymer film upon thermal treatment seems to be totally suppressed.[7,29] The higher value of T_g of PFA-OXD also accounts for the enhanced spectral stability of the polymer film.

Electrochemical Studies. We employed cyclic voltammetry (CV) to investigate the redox behavior of PFA-OXD and to estimate the energy levels of its highest occupied molecular orbital (HOMO) and lowest unoccupied molecular orbital (LUMO). We performed these electrochemical measurements using the polymer film coated on a glassy carbon electrode in an electrolyte of 0.1 M $TBAPF_6$ in acetonitrile and with ferrocene as the internal standard. We attribute the onset potentials at +0.40 and −2.42 V to the oxidation of the fluorene−triphenylamine main chains and the reduction of the OXD side chains, respectively; we estimate the HOMO and LUMO energy levels of PFA-OXD to be −5.20 and −2.38 eV, respectively, with regard to the energy level of ferrocene (4.8 eV below vacuum).[30] The high-lying HOMO levels are in agreement with the data reported previously for copolymers incorporating triarylamine units into the polyfluorene main chains.[13] Relative to the HOMO and LUMO of POF (−5.8 and −2.1 eV, respectively),[10] the higher HOMO energy level of PFA-OXD is better matched to the work function of the ITO/PEDOT electrode (5.2 eV) and, thus, it should facilitate hole injection into the polymer layer from the anode. Moreover, the markedly lower LUMO energy level of PFA-OXD, which originates from the electron-deficient nature of the OXD substituents, indicates that there may be an increase in the electron affinity and an improvement in the electron injection of the polymer.

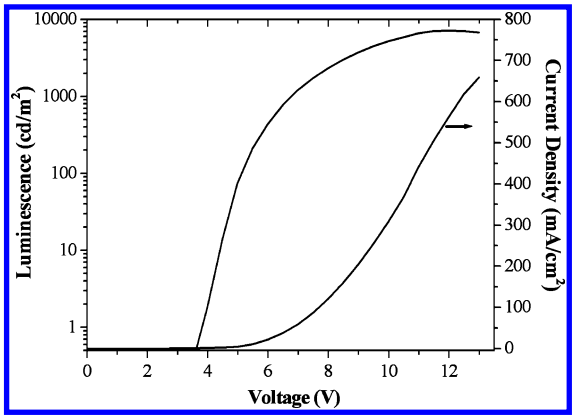

Figure 6. Current density−voltage−luminance characteristics of ITO/PEDOT/PFA-OXD/TPBI/Mg:Ag.

Table 2. Performances of Devices with the Structure ITO/PEDOT/Polymer/TPBI/Mg:Ag

	PFA-OXD	PF-TPA-OXD[d]
turn-on voltage[a] (V)	3.7	4.7
voltage[b] (V)	5.9 (7.7)	7.1 (9.7)
brightness[b] (cd m^{-2})	407 (1966)	295 (1590)
luminance efficiency[b] (cd A^{-1})	2.04 (1.97)	1.46 (1.59)
external quantum efficiency[b] (%)	1.56 (1.51)	1.07 (1.16)
maximum brightness (cd m^{-2})	7128 (at 12 V)	3769 (at 12.5 V)
maximum luminance efficiency (cd A^{-1})	2.07	1.66
maximum external quantum efficiency (%)	1.59	1.21
EL maximum (nm)	461[c]	426[e]
CIE coordinates, x and y	0.14 and 0.15[c]	0.18 and 0.12[e]

[a] At 1 cd m^{-2}. [b] At 20 mA cm^{-2} and the data in parentheses were taken at 100 mA cm^{-2}. [c] At 9 V. [d] Data from ref 31. [e] At 11 V.

Electroluminescence Properties of LED Devices. To evaluate the potential of PFA-OXD to behave as a blue emitter in polymer LED applications, we fabricated devices having the configuration ITO/PEDOT/polymer/TPBI/Mg:Ag. Figure 6 presents the current density−voltage−luminance characteristics of the device employing PFA-OXD as the emitting layer. Because of the low ionization potential of PFA-OXD, which matches well the work function of the ITO/PEDOT electrode, this device turned on at a rather low voltage (3.7 V, corresponding to 1 cd m^{-2}). With the facilitation of hole and electron injection, as well as transport, we obtained the maximum external quantum efficiency of 1.59% at 37.2 mA cm^{-2} (6.5 V) with a brightness of 771 cd m^{-2}; the maximum brightness of 7128 cd m^{-2} occurred at a current density of 563 mA cm^{-2} (12 V). Table 2 summarizes the performance of the PFA-OXD-based device. For the sake of comparison, we include the data of the corresponding device based on PF-TPA-OXD.[31] The PFA-OXD electroluminescence device exhibits much better performance than does the

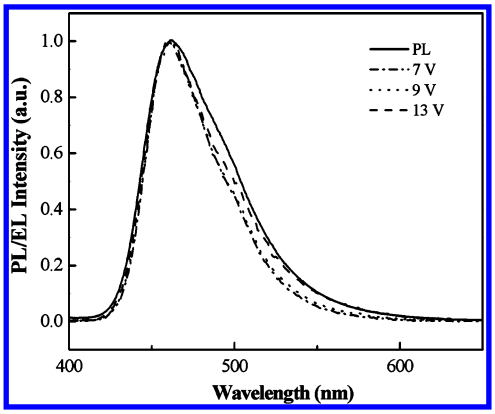

Figure 7. Solid-state PL spectrum of the PFA-OXD film and EL spectra of the ITO/PEDOT/PFA-OXD/TPBI/Mg:Ag devices, recorded at various voltages.

PF-TPA-OXD-based device: it has a lower turn-on voltage, a higher quantum efficiency (η %), and a brighter luminance. It is noteworthy that this PFA-OXD-based device seems to be able to endure a higher current density and to achieve a higher brightness than do other devices employing polyfluorene derivatives as emitters in the same device configuration.[7d,e,31] As indicated in Figure 7, this PFA-OXD-based device exhibits an EL maximum at ca. 460 nm in the resulting spectrum; this value is almost identical with that obtained in the corresponding PL spectrum, which indicates that both the PL and EL originate from the same radiative decay process of the singlet exciton and that no exciplexes formed at the PFA-OXD/TPBI interface. Figure 7 also demonstrates that the PFA-OXD-based device exhibits a voltage-independent and stable EL spectrum. Upon increasing the applied voltages from 7 to 13 V (i.e., beyond the voltage required to achieve maximum brightness), we observed no significant change in the EL spectra; the Commission Internationale de L'Eclairage (CIE) color coordinates at 7 and 13 V were (0.14, 0.14) and (0.15, 0.18), respectively, which fall in the pure-blue region of a CIE chromaticity chart. In contrast, the polydialkylfluorene-based device exhibited an undesirable lower energy emission band between 500 and 600 nm during device operation, turning the pure-blue emission to a blue-green color, i.e., an unstable emission color.[32]

Red Phosphorescence from a Binary Blend. The preparation of electrophosphorescent LEDs utilizing polymers as host materials for the emitting layer is attractive because of the potential for applications in large-area devices prepared using simple solution processing. Efficiently electrophosphorescent polymer-based devices have been prepared by doping PF or poly(*N*-vinylcarbazole) (PVK) with triplet complexes.[4e−h] For the purpose of balancing charges, some electron-transporting materials, such as 2-(4-biphenylyl)-5-(4-*tert*-butylphenyl)-1,3,4-oxadiazole (PBD) and 3-(4-biphenylyl)-4-phenyl-5-(4-*tert*-butylphenyl)-1,2,4-triazole (TAZ), have also been introduced to compensate for the poor ability of the host polymers to transport electrons.[33] Furthermore, devices exhibiting a higher current and brightness, together with lower driving voltages, can be achieved by co-doping with the hole-transporting molecule TPD.[34]

In this study, we used PFA-OXD, which possesses hole-transporting backbones and electron-transporting side chains, as the polymeric host and doped it with a red-emitting phosphorescent dye, Os(fppz), to realize efficient electroluminescence in conjunction with high current and luminance. The observed lifetime of Os(fppz) is 0.7 μs, which is considerably shorter than that of $Ir(btp)_2(acac)$ (5.8 μs).[35] This shorter exciton lifetime may suppress both TT and PT annihilation[36] and lead to improved device quantum efficiency, even at a high current density. As depicted in Figure 8, the PL spectrum of PFA-OXD and the absorption spectrum of Os(fppz) overlap to a moderate extent, which suggests that energy transfer may occur from PFA-OXD to Os(fppz). Figure 9a presents the degree of energy transfer between the PFA-OXD host and Os(fppz) dopant at doping ratios from 0.9 to 4.4 wt % under photoexcitation of the host. Upon excitation of PFA-OXD, the PL profile of the blend contains two emission bands: one centered at ca. 460 nm, which originates from the residual emission of the PFA-OXD host, and the other at ca. 620 nm, which corresponds to the radiative decay from the triplet state of Os(fppz) to the ground state. Even at a higher doping level (4.4 wt %), the PL still displays a significant contribution from the PFA-OXD host. In contrast, the corresponding EL spectra (Figure 9b) indicate that at a doping concentration of 2.6 wt %, the dopant emission dominates completely and results in a red emission having CIE color coordinates of (0.65, 0.34).

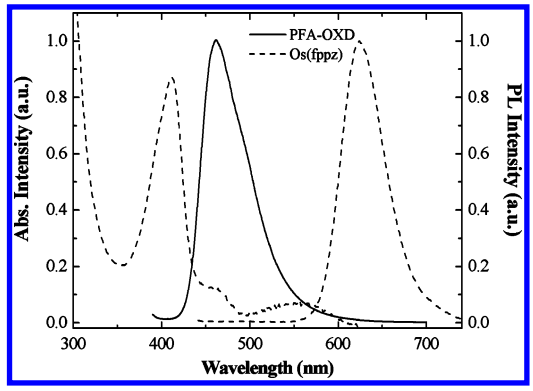

Figure 8. Solid-state PL spectrum of the PFA-OXD film (excited at 380 nm) and the absorption and PL spectra of Os(fppz) (excited at 425 nm) recorded in CH_2Cl_2 solution.

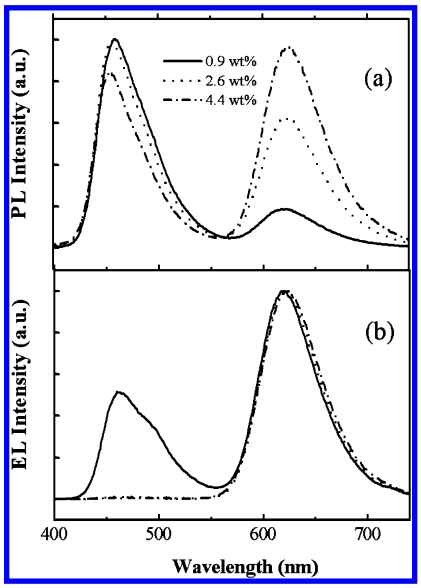

Figure 9. (a) PL (excited at 380 nm) and (b) EL spectra of blends prepared from PFA-OXD doped with different amounts of Os(fppz).

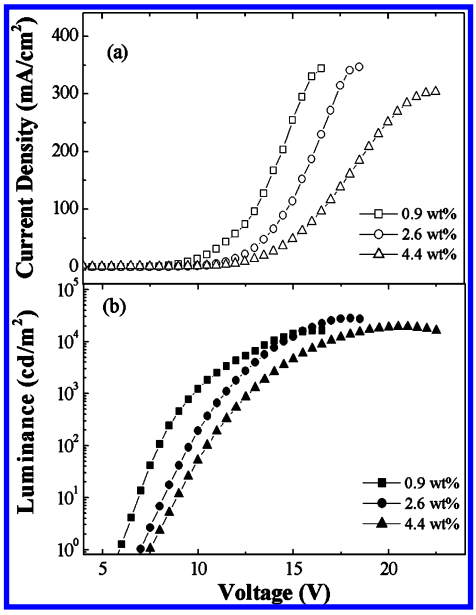

Figure 10. Plots of (a) current density vs applied voltage and (b) luminance vs applied voltage for devices prepared from PFA-OXD doped with different amounts of Os(fppz).

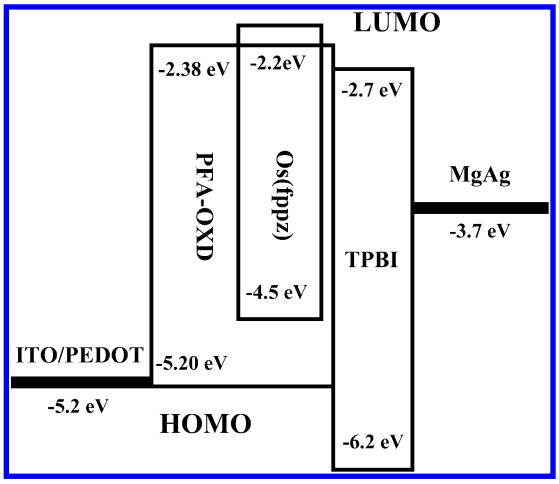

Figure 11. Energy level diagram for devices having the configuration ITO/PEDOT/Os(fppz):PFA-OXD/TPBI/MgAg.

These results suggest that both energy transfer and direct charge trapping/recombination on the Os(fppz) guest are responsible for the observed EL.[4f,g,37] Parts a and b, respectively of Figure 10 present the current density vs voltage ($I-V$) and luminance vs voltage ($L-V$) characteristics of the devices prepared using different amounts of Os(fppz) in PFA-OXD. It is obvious that the operating voltages of the doped devices are higher than those of the nondoped device and that the $I-V$ characteristics shift to higher voltages upon increasing the doping concentration of Os(fppz) in the PFA-OXD host. This result also implies that Os(fppz) moieties serve as charge-trapping sites when dispersed in the PFA-OXD matrix.[4f,g,37] According to the energy level diagram constructed in Figure 11, the HOMO and LUMO levels of Os(fppz) are −4.5 and −2.2 eV, respectively,[16] which indicate that a hole can potentially be trapped at the HOMO of Os(fppz) by a barrier depth of 0.7 eV after injection from the ITO/PEDOT electrode, and can then wait for recombination with an opposite charge (electron) to form excitons. The holes trapped in the Os(fppz) sites would build up a positive space-charge field in the host matrix to impede the further injection of holes from the anode, in turn leading to higher operating voltages.[33a,38] At a doping concentration of 2.6 wt %, the maximum external quantum efficiency of 9.30% occurs at a current density of 5.2 mA cm^{-2} (11 V), together with a brightness of 658 cd m^{-2}. The maximum luminance of 28 440 cd m^{-2} occurred at a current density of 341 mA cm^{-2} (18 V). A further increase in doping concentration to 4.4 wt % resulted in a slight decrease in the external quantum and luminance efficiencies, probably as a result of concentration quenching. We also used atomic force microscopy (AFM) to investigate the phase morphology in the PFA-OXD-Os(fppz) blending system. We observe clearly from the AFM phase image that no phase separation occurred in the 4.4 wt % Os(fppz) doped PFA-OXD film. The root-mean-square surface roughnesses of the pure PFA-OXD film and the 4.4 wt % Os(fppz) doped polymer film were 0.26 and 0.30 nm, respectively. These similar root-mean-square surface roughnesses for the undoped and doped PFA-OXD films support that no detectable phase separation occurred within the blended PFA-OXD-Os(fppz) system.[4f] We infer that the Os complex is dispersed well in PFA-OXD, probably because the polar moieties in PFA-OXD provide a stabilizing environment for the osmium dopant.

Table 3 summarizes the performances of the doped devices that we investigated in this study. The brightness and efficiency of the Os(fppz)-doped devices that we describe in this paper are significantly higher than those we reported previously when employing polyfluorene derivatives containing charge-transporting pendent groups as hosts.[7e,39] Even at a higher current density of 100 mA cm^{-2}, ca. 90% of the peak efficiency was sustained, with a bright phosphorescence emitting from the red-emitting devices. For instance, for the device doped with 2.6 wt % Os(fppz) at a current density of 100 mA cm^{-2}, we obtained an external quantum efficiency of 8.13% in conjunction with a high brightness of 11 036 cd m^{-2}. We attribute the high performance of these Os(fppz)-doped devices, even at higher current

Table 3. Performances of Devices Having the Structure ITO/PEDOT/Os(fppz):PFA-OXD/TPBI/Mg:Ag

Os(fppz) (wt % in PFA-OXD)	0.9 wt %	2.6 wt %	4.4 wt %
turn-on voltage[a] (V)	5.8	7.0	7.5
voltage[b] (V)	10.4 (13.1)	12.4 (14.7)	13.5 (16.6)
brightness[b] (cd m^{-2})	1688 (6825)	2484 (11036)	1919 (9173)
luminance efficiency[b] (cd A^{-1})	8.46 (6.83)	12.42 (11.06)	9.59 (9.18)
external quantum efficiency[b] (%)	5.94 (4.80)	9.13 (8.13)	7.17 (6.86)
maximum brightness (cd m^{-2})	16 395 (at 16 V)	28 440 (at 18 V)	19 264 (at 20.5 V)
maximum luminance efficiency (cd A^{-1})	9.65	12.65	9.71
maximum external quantum efficiency (%)	6.78	9.30	7.26
EL maximum[c] (nm)	620	623	624
CIE coordinates, x and y[c]	0.44 and 0.28	0.65 and 0.34	0.65 and 0.35

[a] At 1 cd m^{-2}. [b] At 20 mA cm^{-2} and the data in parentheses were taken at 100 mA cm^{-2}. [c] At 9 V.

density, to the balanced charge injection and transportation supported by PFA-OXD and the shorter triplet lifetime of Os(fppz); effective exciton confinement within the emitting layer, caused by the hole/exciton blocking (TPBI) layer, could also account for these results.

In conclusion, we have realized a stable blue light emitting polymer, PFA-OXD, which possesses bipolar charge-transporting capability, by incorporating two electron-deficient oxadiazole groups onto the C9 position of each fluorene unit in the hole-transporting fluorene−triphenylamine backbone. From its combination of propeller-like triphenylamine units in the backbones and rigid cardo-type OXD pendent groups, this polymer exhibits a very high glass transition temperature (306 °C) without sacrificing its good solution processability. An EL device based on PFA-OXD displays a stable blue emission having color coordinates of (0.14, 0.15), a maximum brightness of 7128 cd m^{-2}, and a maximum luminance efficiency of 2.07 cd A^{-1}. Moreover, when using PFA-OXD as the host material doped with 2.6 wt % Os(fppz) complex, we realized a high brightness and highly efficient red electroluminescent device having CIE coordinates of (0.65, 0.34), a maximum brightness of 28 440 cd m^{-2}, and a maximum external efficiency of 9.30%. Even at a higher current density (100 mA cm^{-2}), the device maintains a high efficiency (8.13%) with brightness exceeding 10^4 cd m^{-2}.

Acknowledgment. We thank the National Science Council for financial support. Our special thanks go to Prof. C.-H. Cheng, Dr. J.-P. Duan, and Dr. H.-T. Shih for their support and cooperation during the preparation and characterization of the light-emitting devices.

References and Notes

(1) Mitschke, U.; Bäurele, P. *J. Mater. Chem.* **2000**, *10*, 1471.

(2) (a) Kraft, A.; Grimsdale, A. C.; Holmes, A. B. *Angew. Chem., Int. Ed.* **1998**, *37*, 402. (b) Friend, R. H.; Gymer, R. W.; Holmes, A. B.; Burroughes, J. H.; Marks, R. N.; Taliani, C.; Bradley, D. D. C.; Dos Santos, D. A.; Brédas, J. L.; Lögdlund, M.; Salaneck, W. R. *Nature* **1999**, *397*, 121. (c) Bernius, M. T.; Inbasekaran, M.; O'Brien, J.; Wu, W. *Adv. Mater.* **2000**, *12*, 1737.

(3) (a) Morin, J.-F.; Leclerc, M. *Macromolecules* **2002**, *35*, 8413. (b) Müller, C. D.; Falcou, A.; Reckefuss, N.; Rojahn, M.; Wiederhirn, V.; Rudati, P.; Frohne, H.; Nuyken, O.; Becker, H.; Meerholz, K. *Nature* **2003**, *241*, 829. (c) Ego, C.; Marsitzky, D.; Becker, S.; Zhang, J.; Grimsdale, A. C.; Müllen, K.; MacKenzie, J. D.; Silva, C.; Friend, R. H. *J. Am. Chem. Soc.* **2003**, *125*, 437. (d) Yang, R.; Tian, R.; Yang, Y.; Hou, Q.; Cao, Y. *Macromolecules* **2003**, *36*, 7453. (e) Niu, Y.-H.; Hou, Q.; Cao, Y. *Appl. Phys. Lett.* **2003**, *82*, 2163. (f) Niu, Y.-H.; Huang, J.; Cao, Y. *Adv. Mater.* **2003**, *15*, 807. (g) Yang, J.; Jiang, C.; Zhang, Y.; Yang, R.; Yang, W.; Hou, Q.; Cao, Y. *Macromolecules* **2004**, *37*, 1211. (h) Yang, R.; Tian, R.; Yan, J.; Zhang, Y.; Yang, J.; Hou, Q.; Yang, W.; Zhang, C.; Cao, Y. *Macromolecules* **2005**, *38*, 244.

(4) (a) Kido, J.; Hongawa, K.; Okuyama, K.; Nagai, K. *Appl. Phys. Lett.* **1994**, *64*, 815. (b) Kido, J.; Shionoya, H.; Nagai, K. *Appl. Phys. Lett.* **1995**, *67*, 2281. (c) Lee, J.-I.; Kang, I.-N.; Hwang, D.-H.; Shim, H.-K.; Jeoung, S. C.; Kim, D. *Chem. Mater.* **1996**, *8*, 1925. (d) McGehee, M. D.; Bergstedt, T.; Zhang, C.; Saab, A. P.; O'Regan, M. B.; Bazan, G. C.; Srdanov, V. I.; Heeger, A. J. *Adv. Mater.* **1999**, *11*, 1349. (e) Gong, X.; Robinson, M. R.; Ostrowski, J. C.; Moses, D.; Bazan, G. C.; Heeger, A. J. *Adv. Mater.* **2002**, *14*, 581. (f) Chen, F.-C.; Chang, S.-C.; He, G.; Pyo, S.; Yang, Y.; Kurotaki, M.; Kido, J. *J. Polym. Sci., Part B: Polym. Phys.* **2003**, *41*, 2681. (g) Noh, Y.-Y.; Lee, C.-L.; Kim, J.-J.; Yase, K. *J. Chem. Phys.* **2003**, *118*, 2853. (h) Chen, F.-C.; He, G.; Yang, Y. *Appl. Phys. Lett.* **2003**, *82*, 1006. (i) Kim, J.-H.; Liu, M. S.; Jen, A. K.-J.; Carlson, B.; Dalton, L. R.; Shu, C.-F.; Dodda, R. *Appl. Phys. Lett*. **2003**, *83*, 776. (j) Kim, J.-H.; Herguth, P.; Kang, M.-S.; Jen, A. K.-Y.; Tseng, Y.-H.; Shu, C.-F. *Appl. Phys. Lett.* **2004**, *85*, 1116. (k) Niu, Y.-H.; Chen, B.; Liu, S.; Yip, H.; Bardecker, J.; Jen, A. K.-Y.; Kavitha, J.; Chi, Y.; Shu, C.-F.; Tseng, Y.-H.; Chien, C.-H. *Appl. Phys. Lett.* **2004**, *85*, 1619. (l) Niu, Y.-H.; Tung, Y.-L.; Chi, Y.; Shu, C.-F.; Kim, J. H.; Chen, B.; Luo, J.; Carty, A. J.; Jen, A. K.-Y. *Chem. Mater.* **2005**, *17*, 3532.

(5) (a) Pei, Q.; Yang, Y. *J. Am. Chem. Soc.* **1996**, *118*, 7416. (b) Kreyenschmidt, M.; Klaerner, G.; Fuhrer, T.; Ashenhurst, J.; Karg, S.; Chen, W. D.; Lee, V. Y.; Scoot, J. C.; Miller, R. D. *Macromolecules* **1998**, *31*, 1099. (c) Leclerc, M. *J. Polym. Sci., Part A: Polym. Chem.* **2001**, *39*, 2867. (d) Neher, D. *Macromol. Rapid Commun.* **2001**, *22*, 1365. (e) Becker, S.; Ego, C.; Grimsdale, A. C.; List, E. J. W.; Marsitzky, D.; Pogantsch, A.; Setayesh, S.; Leising, G.; Müllen, K. *Synth. Met.* **2002**, *125*, 73.

(6) Teetsov, J.; Fox, M. A. *J. Mater. Chem.* **1999**, *9*, 2117.

(7) (a) Ego, C.; Grimsdale, A. C.; Uckert, F.; Yu, G.; Srdanov, G.; Müllen, K. *Adv. Mater.* **2002**, *14*, 809. (b) Wu, F.-I.; Reddy, D. S.; Shu, C.-F.; Liu, M. S.; Jen, A. K.-Y. *Chem. Mater.* **2003**, *15*, 269. (c) Shu, C.-F.; Dodda, R.; Wu, F.-I.; Liu, M. S.; Jen, A. K.-Y. *Macromolecules* **2003**, *36*, 6698. (d) Su, H.-J.; Wu, F.-I.; Shu, C.-F. *Macromolecules* **2004**, *37*, 7197. (e) Su, H.-J.; Wu, F.-I.; Shu, C.-F.; Tung, Y.-L.; Chi, Y.; Lee, G.-H. *J. Polym. Sci., Part A: Polym. Chem.* **2005**, *43*, 859.

(8) (a) Xia, C.; Advincula, R. C. *Macromolecules* **2001**, *34*, 5854. (b) Vamvounis, G.; Schulz, G. L.; Holdcroft, S. *Macromolecules* **2004**, *37*, 8897. (c) Kulkarni, A. P.; Zhu, Y.; Jenekhe, S. A. *Macromolecules* **2005**, *38*, 1553.

(9) (a) List, E. J. W.; Guentner, R.; De Freitas, P. S.; Scherf, U. *Adv. Mater.* **2002**, *14*, 374. (b) Romaner, L.; Pogantsch, A.; De Freitas, P. S.; Scherf, U.; Gaal, M.; Zojer, E.; List, E. J. W. *Adv. Funct. Mater.* **2003**, *13*, 597.

(10) Janietz, S.; Bradley, D. D. C.; Grell, M.; Giebeler, C.; Inbasekaran, M.; Woo, E. P. *Appl. Phys. Lett.* **1998**, *73*, 2453.

(11) Brown, T. M.; Kim, J. S.; Friend, R. H.; Cacialli, F.; Daik, R.; Feast, W. J. *Appl. Phys. Lett.* **1999**, *75*, 1679.

(12) Sainova, D.; Miteva, T.; Nothofer, H. G.; Scherf, U.; Glowacki, I.; Ulanski, J.; Fujikawa, H.; Neher, D. *Appl. Phys. Lett.* **2000**, *76*, 1810.

(13) Bernius, M.; Inbasekaran, M.; Woo, E.; Wu, W.; Wujkowski, L. *J. Mater. Sci.: Mater. Electron.* **2000**, *11*, 111.

(14) (a) Palilis, L. C.; Lidzey, D. G.; Redecker, M.; Bradley, D. D. C.; Inbasekaran, M.; Woo, E. P.; Wu, W. W. *Synth. Met.* **2000**, *111*−*112*, 159. (b) Woo, E. P.; Bernius, M. T.; Inbasekaran, M.; Wu, W. U.S. Patent 6,309,763, 2001.

(15) Redecker, M.; Bradley, D. D. C.; Inbasekaran, M.; Wu, W. W.; Woo, E. P. *Adv. Mater.* **1999**, *11*, 241.

(16) Tung, Y.-L.; Wu, P.-C.; Liu, C.-S.; Chi, Y.; Yu, J.-K.; Hu, Y.-H.; Chou, P.-T.; Peng, S.-M.; Lee, G.-H.; Tao, Y.; Carty, A. J.; Shu, C.-F.; Wu, F.-I. *Organometallics* **2004**, *23*, 3745.

(17) Wenseleers, W.; Stellacci, F.; Meyer-Friedrichsen, T.; Mangel, T.; Bauer, C. A.; Pond, S. J. K.; Marder, S. R.; Perry, J. W. *J. Phys. Chem. B* **2002**, *106*, 6853.

(18) Shi, J.; Tang, C. W.; Chen, C. H. U.S. Patent 5,645,948, 1997.

(19) Culligan, S. W.; Geng, Y.; Chen, S. H.; Klubek, K.; Vaeth, K. M.; Tang, C. W. *Adv. Mater.* **2003**, *15*, 1176.

(20) Kodomari, M.; Satoh, H.; Yoshitomi, S. *J. Org. Chem.* **1988**, *53*, 2093.

(21) Miyaura, N.; Suzuki, A. *Chem. Rev.* **1995**, *95*, 2457.

(22) (a) Liou, G.-S.; Hsiao, S.-H. *J. Polym. Sci., Part A: Polym. Chem.* **2003**, *41*, 94. (b) Sancho-Garaía, J. C.; Foden, C. L.; Grizzi, I.; Greczynski, G.; De Jong, M. P.; Salaneck, W. R.; Brédas, J. L.; Cornil, J. *J. Phys. Chem. B* **2004**, *108*, 5594. (c) Chen, S.-H.; Hsiao, S.-H.; Su, T.-H.; Liou, G.-S. *Macromolecules* **2005**, *38*, 307.

(23) (a) Yu, G.; Liu, Y.; Wu, X.; Zheng, M.; Bai, F.; Zhu, D.; Jin, L.; Wang, M. Wu, X. *Appl. Phys. Lett.* **1999**, *74*, 2295. (b) Huang, H.; He, Q.; Song, Y.; Lin, H.; Yang, J.; Bai, F. *Polym. Adv. Technol.* **2003**, *14*, 309.

(24) Wyszecki, G.; Stiles, W. S. *Color Science: Concepts and Methods, Quantitative Data and Formulae*; John Wiley & Sons: New York, 1982; p 259.

(25) Li, Y.; Ding, J.; Day, M.; Tao, Y.; Lu, J.; D'iorio, M. *Chem. Mater.* **2004**, *16*, 2165.

(26) Turro, N. J. *Modern Molecular Photochemistry*; University Science Books: Sausalito, CA, 1991.

(27) Eaton, D. *Pure Appl. Chem.* **1998**, *60*, 1107.

(28) Grice, A. W.; Bradley, D. D. C.; Bernius, M. T.; Inbasekaran, M.; Wu, W. W.; Woo, E. P. *Appl. Phys. Lett.* **1998**, *73*, 629.

(29) Bliznyuk, V. N.; Carter, S. A.; Scott, J. C.; Klärner, G.; Miller, R. D.; Miller, D. C. *Macromolecules* **1999**, *32*, 361.

(30) Pommerehne, J.; Vestweber, H.; Guss, W.; Mahrt, R. F.; Bässler, H.; Porsch, M.; Daub, J. *Adv. Mater.* **1995**, *7*, 551.
(31) Su, H.-J.; Wu, F.-I.; Tseng, Y.-H.; Shu, C.-F. *Adv. Funct. Mater.* **2005**, *15*, 1209.
(32) Weinfurtner, K.-H.; Fujikawa, H.; Tokito, S.; Taga, Y. *Appl. Phys. Lett.* **2000**, *76*, 2502.
(33) (a) Yang, X.; Neher, D.; Hertel, D.; Däubler, T. K. *Adv. Mater.* **2004**, *16*, 161. (b) Jiang, C.; Yang, W.; Peng, J.; Xiao, S.; Cao, Y. *Adv. Mater.* **2004**, *16*, 537.
(34) Yang, X. H.; Neher, D. *Appl. Phys. Lett.* **2004**, *84*, 2476.
(35) Lamansky, S.; Djurovich, P.; Murphy, D.; Abdel-Razzaq, F.; Lee, H.-E.; Adachi, C.; Burrows, P. E.; Forrest, S. R.; Thompson, M. E. *J. Am. Chem. Soc.* **2001**, *123*, 4304.
(36) (a) Baldo, M. A.; Adachi, C.; Forrest, S. R. *Phys. Rev. B* **2000**, *62*, 10967. (b) Chen, F.-C.; Yang, Y.; Thompson, M. E.; Kido, J. *Appl. Phys. Lett.* **2002**, *80*, 2308.
(37) Uchida, M.; Adachi, C.; Koyama, T.; Taniguchi, Y. *J. Appl. Phys.* **1999**, *86*, 1680.
(38) (a) Virgili, T.; Lidzey, D. C.; Bradley, D. D. C. *Synth. Met.* **2000**, *111*−*112*, 203. (b) O'Brien, D. F.; Giebeler, C.; Fletcher, R. B.; Cadlby, A. J.; Palilis, L. C.; Lidzey, D. C.; Lane, P. A.; Bradley, D. D. C.; Blau, W. *Synth. Met.* **2001**, *116*, 379.
(39) Wu, F.-I.; Shih, P.-I.; Tseng, Y.-H.; Chen, G.-Y.; Chien, C.-H.; Shu, C.-F.; Tung, Y.-L.; Chi, Y.; Jen, A. K.-Y. *J. Phys. Chem. B* **2005**, *109*, 14000.

MA051842R